ACS APPLIED MATERIALS & INTERFACES

Research Article

www.acsami.org

Ultrananocrystalline Diamond-Decorated Silicon Nanowire Field Emitters

Javier Palomino,*[,†,‡] Deepak Varshney,[†,‡] Oscar Resto,[‡] Brad R. Weiner,[†,§] and Gerardo Morell[†,‡]

[†]Institute of Functional Nanomaterials, University of Puerto Rico, San Juan, PR 00931, United States

[‡]Department of Physics and [§]Department of Chemistry, University of Puerto Rico, San Juan, PR 00936, United States

ABSTRACT: Silicon nanowires (SiNWs) were uniformly decorated with ultrananocrystalline diamond (UNCD) by a novel route using paraffin wax as the seeding source, which is more efficient in the creation of diamond nuclei than traditional methods. These one-dimensional ultrananocrystalline diamond-decorated SiNWs (UNCD/SiNWs) exhibit uniform diameters ranging from 100 to 200 nm with a bulbous catalytic tip of ∼250 nm in diameter and an UNCD grain size of ∼5 nm. UNCD/SiNW nanostructures demonstrated enhanced electron field emission (EFE) properties with a turn-on field of about 3.7 V/μm. Current densities around 2 mA/cm^2 were achieved at 25 V/μm, which is significantly enhanced as compared to bare SiNWs.

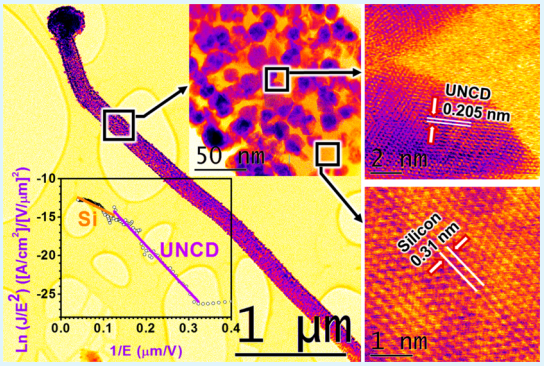

KEYWORDS: *silicon nanowires, ultrananocrystalline diamond, electron field emission*

1. INTRODUCTION

One-dimensional nanostructures, such as nanotubes and nanowires, have been extensively studied because of their novel physical and chemical properties and their potential applications in device development.[1−3] One-dimensional silicon nanowires (SiNWs) were first fabricated via a vapor−liquid−solid (VLS) mechanism,[4] followed by other approaches, such as chemical vapor deposition,[1] laser ablation,[2] thermal evaporation,[3] and chemical etching.[5] Fabrication of electron-emitting nanomaterials[6−8] and their application to flat panel displays[9,10] has attracted much attention to the study of one-dimensional materials having high aspect ratio, stable structure, and high electron field emission (EFE) properties.[11−15] Because silicon plays a significant role in the microelectronic field, SiNW-based emitters[16,17] have been widely studied. To improve the EFE property, various kinds of modifications have been done on SiNWs, such as H_2 plasma surface treatment,[18] Mo modification,[19] Ni implantation,[20] IrO_2 coating,[21] gold decoration,[22] and diamond coating.[23−26]

Diamond films have been widely studied for use in electron field emitters in vacuum microelectronic devices because of their negative electron affinity (NEA) with low effective work function.[27] However, the electron field emission properties of diamond are inferior to those of SiNWs[18] because its conduction band is empty at room temperature due to its wide bandgap. Numerous approaches have been developed to enhance the electron field emission properties of diamond films, including the modification of grain shape, reduction of grain size,[28] increasing the conductivity by doping with boron and nitrogen species,[29] and fabricating diamond tips through the utilization of high aspect ratio templates.[30] Aligned silicon tip arrays, which have been used as templates for synthesizing diamond tips, were prepared by employing the conventional chemical vapor deposition, electron beam lithography, and chemical etching techniques, along with the microelectronic processes.[23,31−33] However, these approaches require a sophisticated apparatus and complex processing steps, which are tedious and expensive. On the other hand, building upon the valuable reported information related to diamond and SiNWs and the expertise of our group in the growth of ultrananocrystalline diamond (UNCD) using paraffin wax,[34] we hereby present UNCD/SiNW nanostructures as upgraded electron field emitters.

2. EXPERIMENTAL PROCEDURE

Step I. Fabrication of SiNWs. The first step of the experimental process constitutes the fabrication of SiNWs, for which a copper substrate was coated with a thin gold layer (100−200 nm) using the radio frequency (RF) sputtering technique, which acts as a catalyst to grow SiNWs. Thereby, the source material consisting of a mixture of Si nanoparticles and graphite (1:1) was placed at the center of a quartz tube (1050 °C) in a custom-built thermal CVD system, whereas the gold-coated copper substrate was placed at the downstream side of the Ar flow, 7−10 cm away (950 °C) from the source material, as shown by Figure 1. In contact with graphite at high temperature, the native SiO_x is reduced to form Si and CO_x vapors. A continuous flow (100 sccm) of argon gas was introduced from one closed end of the quartz tube serving as a carrier gas. The temperature of the source material was first raised from room temperature to 1050 °C and kept within this temperature range for 3 h until the end of the growth process, keeping a constant pressure of 100 mT.

Received: May 24, 2014
Accepted: July 21, 2014
Published: July 21, 2014

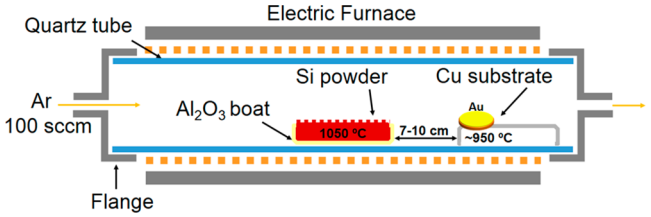

Figure 1. Schematic representation of the thermal CVD system showing the configuration of raw materials and the corresponding temperatures.

Step II. UNCD Coating on SiNWs. In the second step, the SiNWs were coated with UNCD by using a hot filament chemical vapor deposition (HFCVD) process. The SiNWs were first coated with melted paraffin wax that was used as a seeding source. Under the HFCVD conditions, the paraffin wax decomposes, leaving behind abundant sp^3-C crystallites[34] on the SiNW surface that result in enhanced nucleation of UNCD. Paraffin wax is more efficient in the creation of diamond nuclei than traditional detrimental methods, such as polishing and ultrasonication, which produce substantial surface damage. The deposition of UNCD was carried out in a gas mixture consisting of 0.3% CH_4 and 99.7% H_2. The pressure and flow rate were maintained at 20 Torr (2.7×10^3 Pa) and 100 sccm, respectively. The growth process was carried out at relatively low temperatures (~400−500 °C).[35]

Characterization Methods. The morphology of the fabricated films was examined by using a JEOL JSM-7500F field emission scanning electron microscope (FESEM) and JEOL JEM-2200FS high-resolution transmission electron microscopy (HRTEM). The films were also characterized by Raman spectroscopy performed at room temperature, using a Jobin-Yvon T6400 spectrometer and 514 nm Ar-ion laser as the excitation source. The EFE characteristics of the films were measured using a Stanford Research Systems PS350 power supply and Keithley 6517A electrometer. All the measurements were recorded at an anode−cathode distance, d_{CA} = 100 ± 2 μm, and at a pressure of ~5×10^{-7} Torr (6.7×10^{-5} Pa). Currents lower than 1×10^{-12} A were assumed as background noise. Labview was employed to make multiple data acquisitions and calculate the average response. Only results that are consistently reproducible are hereby reported. The details of the measurement setup and procedures involved have been reported elsewhere.[36]

3. RESULTS AND DISCUSSION

The field emission scanning electron microscopic (FESEM) images (Figure 2) reveal the morphology of the bare SiNWs and UNCD-decorated SiNWs. Figure 2a shows uniform and high density growth of bare Si nanowires, where the diameter of the nanowire estimated from the present image falls in the range of 80−160 nm and the tip of each wire is bulbous of about 180−250 nm suggesting the presence of (Au) catalyst at the apex and pointing to a VLS growth mechanism. Figure 2b shows a low-magnification image of high density growth of UNCD-coated Si nanowires. Figure 2c shows the uniform UNCD coating on SiNWs obtained using paraffin wax as diamond seed, indicating that the paraffin wax on the as-grown SiNW acts as diamond nuclei in the HFCVD environment. The UNCD coating is exceptionally uniform throughout the wire length, as compared to published reports.[24,25,32] The magnified image of a single nanowire also shows a uniformly UNCD-coated bulbous tip (shown in Figure 2d).

The room-temperature Raman spectrum of the UNCD-coated Si nanowires is shown in Figure 3. It was taken in the range from 100 to 2000 cm^{-1}, revealing a strong first-order Si transverse optical phonon mode (TO) at 514 cm^{-1}. The symmetric and high intensity peak indicates the high

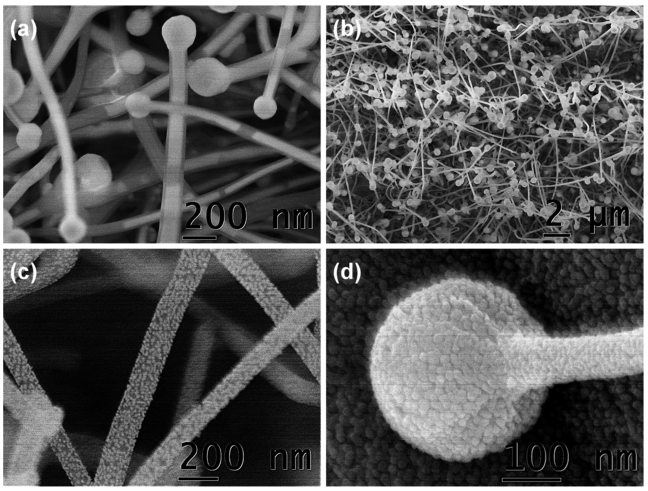

Figure 2. SEM images of the as-grown (a) core/shell structure SiNW/SiO_x showing (Au) catalyst at its tip. (b) High density of UNCD/SiNWs at low magnification, (c) UNCD uniformly coated SiNWs, and (d) apex at high magnification.

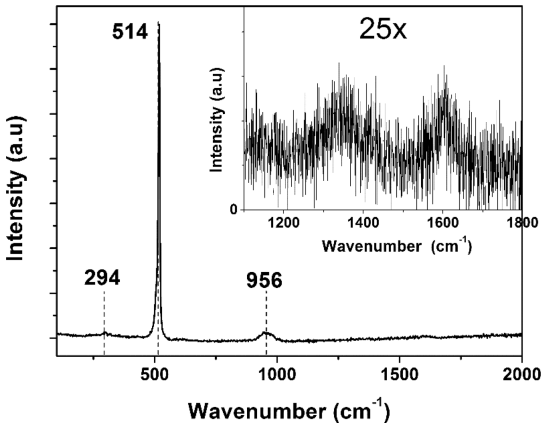

Figure 3. Raman spectrum of UNCD-coated SiNWs. Inset shows the spectrum in the range of 1000−2000 cm^{-1} for UNCD.

crystallinity of the NWs.[37] Compared to bulk Si (521 cm^{-1}), a downshift is observed for the samples, which is not caused by the phonon confinement effect,[38] since the diameter of the SiNWs is relatively large as compared to the excitonic Bohr radius of Si. Hence, the redshift can be attributed to the tensile strain experienced by the NWs[39] due to the coating (shown in Figure 2). In addition, there are two small and broad peaks at around 925 and 290 cm^{-1} corresponding to the second-order transverse optical (2TO) and acoustic (TA) phonon modes of Si, respectively.[40] The inset of Figure 3 (magnified by 25×) shows the typical visible Raman spectrum of UNCD[41] coating over SiNWs[25] in the range from 1000 to 2000 cm^{-1}, revealing a broad D band around 1347 cm^{-1} arising from a disordered sp^2 carbon[41] present at the UNCD grain boundaries. The Raman cross section of Si is much higher than that of diamond, accounting for the relative intensities. The broadening of the D peak can be attributed to the phonon confinement effect due to the small grain size of UNCD (~5 nm).[42] The highly optically absorbing sp^2-bonded carbon precludes observation of the sp^3 Raman signal since the visible Raman is about 50−250 times more sensitive to sp^2-bonded carbon than to the sp^3-bonded carbon.[43] The band around 1600 cm^{-1} corresponds to sp^2-

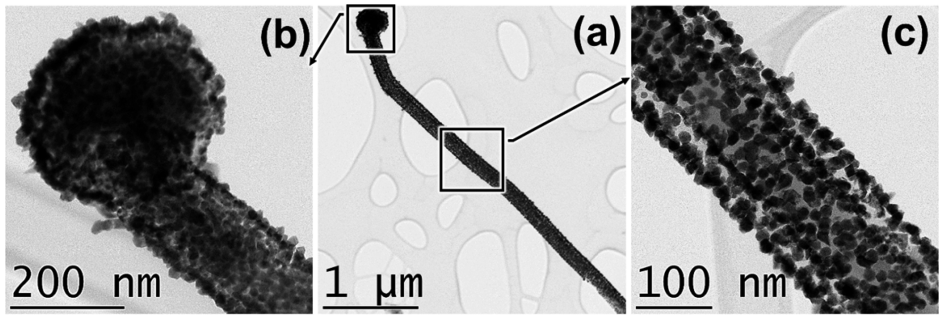

Figure 4. TEM images of (a) UNCD-coated Si NW, (b) bulbous tip of the wire, and (c) linear part of the wire.

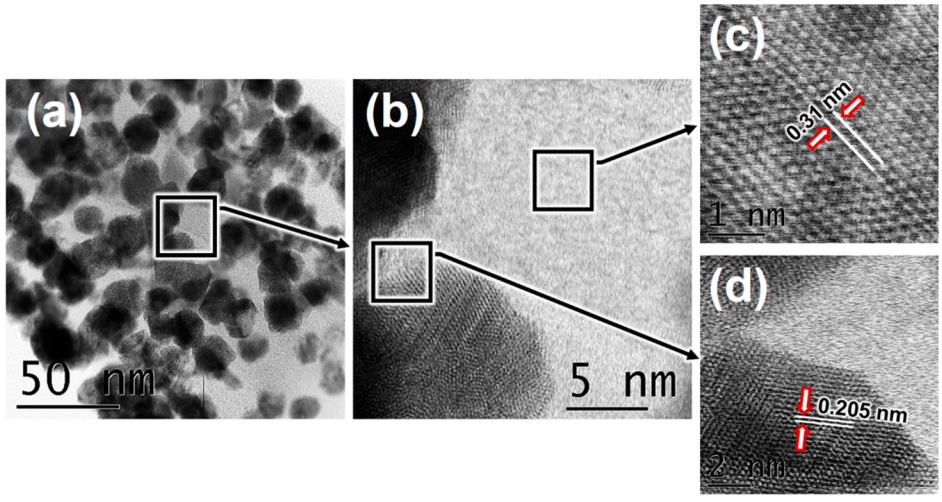

Figure 5. High-resolution transmission electron microscopic scanning mode (STEM) images of (a) UNCD-coated SiNW and (b) magnified image of the wire showing (c) interplanar spacing of the Si crystal and (d) diamond crystals.

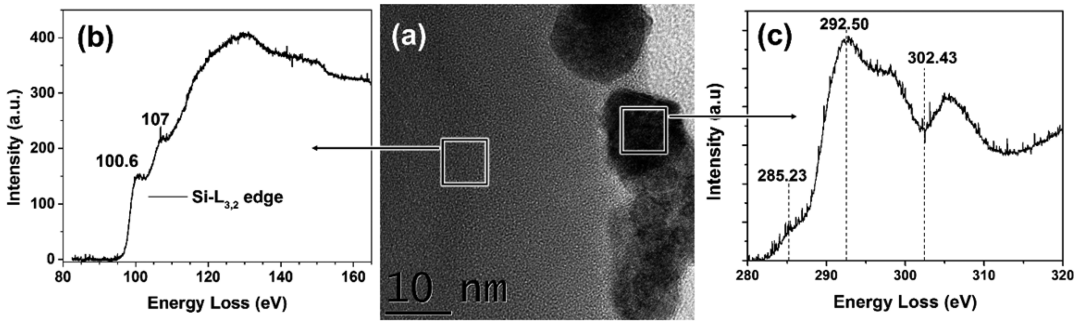

Figure 6. Electron energy loss spectra (EELS) of (b) SiNWs and (c) UNCD crystals recorded at the region shown in (a).

hybridized carbon indicating the presence of graphitic carbon accumulated at the grain boundaries.[44]

Examination of nanoparticles using transmission electron microscopy (TEM) and electron energy loss spectroscopy (EELS) is necessary to unambiguously identify the nature of the material. Figure 4 shows TEM images of the UNCD-decorated SiNWs revealing that they are uniformly coated with dense nanoparticles (UNCD crystals). Figure 4a shows a constant diameter wire, which consists of a core−shell structure with numerous nanosized particles of sizes ranging from 3 to 10 nm dispersed uniformly over the shell along the whole wire. Figure 4b shows a magnified image of the bulbous wire tip revealing that it is also covered with UNCD nanoparticles. Figure 4c is a magnified image of the linear portion of the UNCD/SiNW that clearly reveals the core−shell structure of the SiNW having a UNCD shell thickness of around 10−20 nm.

Figure 5a depicts the HRTEM micrograph of UNCD grown on SiNWs, suggesting that the UNCD is comprised of very small grains (~5 nm). On further magnification (Figure 5b), the crystalline core−shell structure of the wire with uniform coating of UNCD crystals is clearly observed. Figure 5c shows the lattice fringes of the nanowire crystalline core, revealing an interplanar spacing of about 0.31 nm, which matches with the (111) orientation of Si and is consistent with the published data.[45] The HRTEM image of the wires coated with UNCD particles is shown in Figure 5d, indicating that the lattice spacing is about 0.205 nm, which is a typical lattice parameter for diamond,[33] consistent with the diamond (111) planes. The

data were obtained by HRTEM measurements and subsequent calculations on the digital micrograph.

We further explored the UNCD by EELS, which is very sensitive to the local chemical bonding of carbon, and it was carried out (using a beam size of 20 nm) on different regions (see Figure 6). The EELS spectrum was recorded for the nanowire core (shown in Figure 6a), and it exhibits distinct and well-established spectral features of Si in the range of 100−160 eV, as shown in Figure 6b. The small peak at 107 eV is attributed to the presence of SiO_x[46] coming from atmospheric contamination. On the other hand, Figure 6c was recorded for UNCD coating showing the presence of a weak band feature at 285.23 eV, corresponding to the C 1s → π^* transition and indicating the presence of sp^2-C, in agreement with the Raman spectrum discussed above. Moreover, it shows that the C 1s→ σ^* transition around 292.3 eV is consistent with sp^3-bonded carbon[47] and a dip at ∼302.4 eV corresponding to the second absolute band gap of diamond that confirms the diamond nature of the nanograins.[48]

Energy-dispersive spectroscopic (EDS) elemental mapping (Figure 7) was carried out to study the spatial distribution of Si,

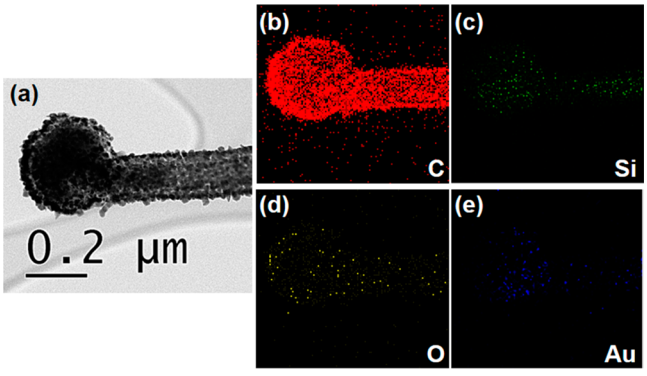

Figure 7. EDS color mapping of (a) UNCD-coated SiNW, with the elemental composition for (b) carbon, (c) silicon, (d) oxygen, and (e) gold.

Au, O, and C on the UNCD-coated SiNWs. Figure 7a is the TEM morphological image of a representative wire, and Figure 7b−e shows its mapping-elemental analysis. Figure 7b reveals a strong signal of C indicating a high density, uniform coating of UNCD throughout the wire as well as the tip. The Si elemental distribution profile points out that the elemental Si is located mostly in the middle region (core) as compared to the edge area (shell). The low intensity signals detected in the core region (Figure 7c) are due to the spherical geometry of the shell covered wires. O is mainly distributed in the shell region of the wires (Figure 7d), which is ascribed to the SiO_x shell, while Figure 7e reveals that elemental gold is mainly distributed at the tip of the NW, which again confirms the VLS[4] mechanism of the Si nanowire growth. The elemental analysis indicates that the Si nanowires are coated with SiO_x and UNCD, forming core/shell heterostructure. This result is consistent with the observed bright/dark contrast in the TEM images discussed above.

From the various characterization results obtained, viz., SEM, TEM, HRTEM, and EDS color mapping, we propose a qualitative mechanism involving the growth of UNCD-coated Si nanowires.

For Si Nanowire Growth. The synthesis of Si nanowires follows the VLS[4,49] growth mechanism, with Au as the catalyst in the present case. Figure 8 shows a schematic representation of the VLS mechanism, where the metal (Au) catalyst thin film

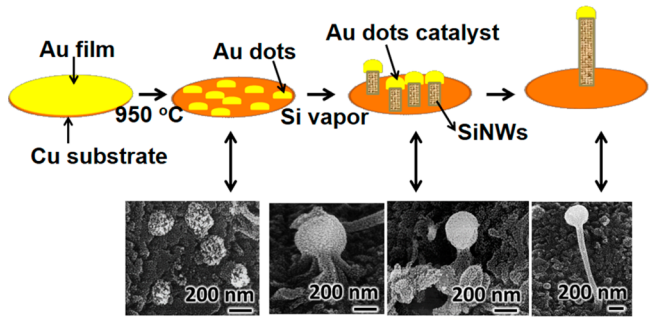

Figure 8. Schematic representation of the VLS growth mechanism of SiNWs, supported with FESEM images.

forms liquid Au−Si alloy droplets at high temperatures (950 °C) that adsorb vapors of source material (Si) achieving a super saturation stage, and the subsequent precipitation of the source material (Si) at the liquid−solid interface occurs to accomplish the minimum free energy of the alloy system. Therefore, the 1D crystal growth begins, and it continues as long as the vapor components are supplied. Since vapor (carrying Si nanoparticles), liquid (gold catalyst), and solid (precipitated one-dimensional structures) phases are involved, it is known as the VLS mechanism.[4,49,50]

For Diamond Growth. Figure 9 shows the schematic representation of the UNCD growth on SiNW seeded by

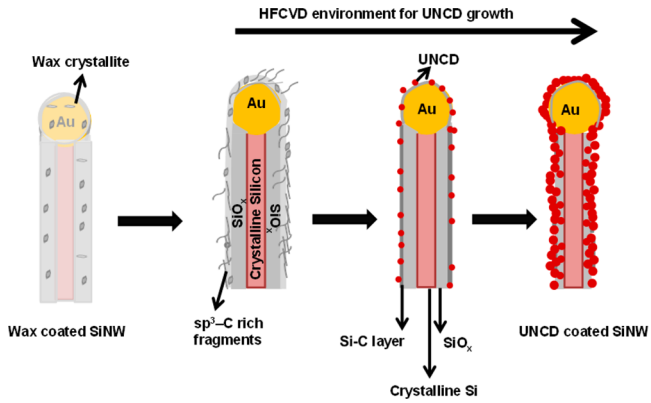

Figure 9. Schematic representation of the growth mechanism of UNCD on SiNWs.

paraffin wax. Decomposition of paraffin wax produces large amounts of sp^3-C rich nanofragments that result in enhanced nucleation of UNCD. These active nuclei are ready for reacting with carbon species in the HFCVD environment to produce UNCD.[51] Two factors limit the ability of the nanodiamond grains to grow beyond 5−10 nm, the three-dimensional network structure of the Si nanowires and the presence of silicon oxide remnants. On flat Cu substrates, on the other hand, similar parameters can yield nanodiamond grains of 10−15 nm.[34]

Moreover, the thin SiO_x layer on the wires together with the presence of sp^3-C rich environment may also play an important role. Active Si sites are generated from the reduction of the SiO_2 layer under the assistance of hydrogen atoms.[52] This leads

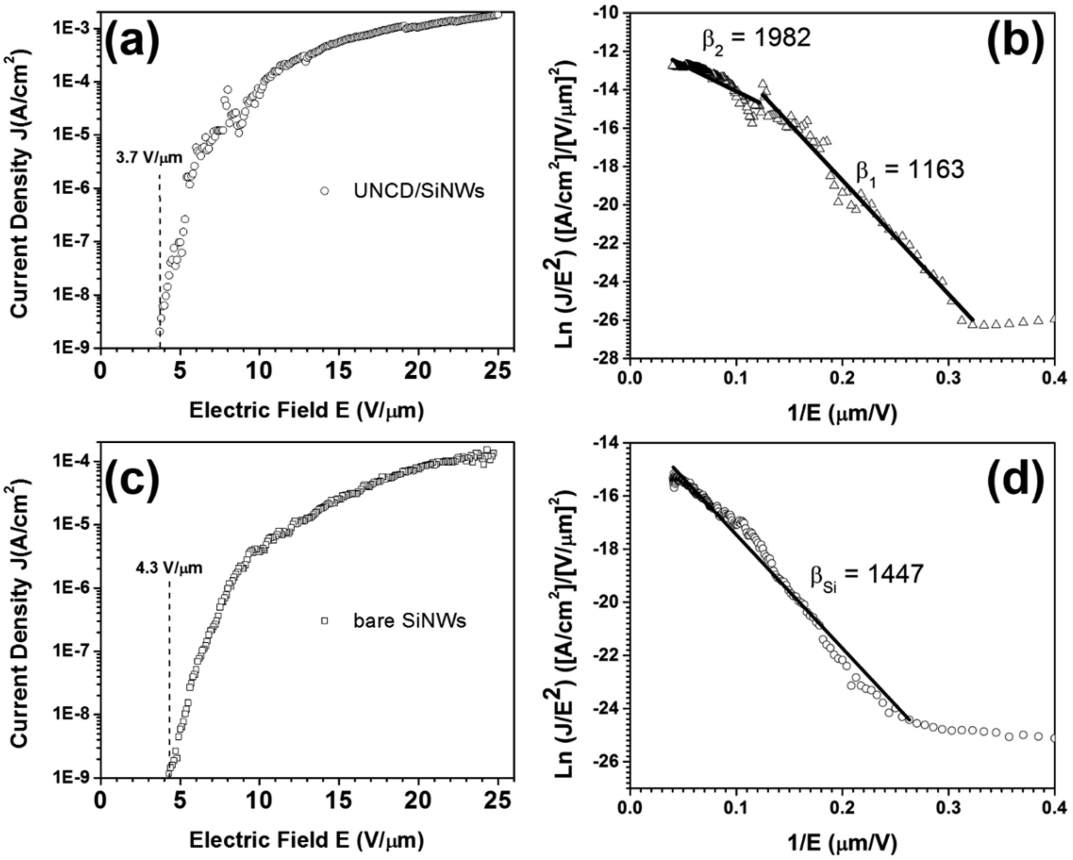

Figure 10. Field emission $J-E$ plots at a cathode−anode distance of about 100 μm: (a) UNCD/SiNWs film and (c) as-grown SiNWs. Fowler−Nordheim $\ln(J/E^2)$ vs $(1/E)$ plots: (b) UNCD/SiNWs film and (d) as-grown SiNWs.

to the formation of a Si−C interfacial layer that also acts as a nucleation site for UNCD growth.[31,32,48]

Field emission measurements were carried out at room temperature after conditioning the films at around 10 μA at their respective field for about 2 h. The measured current density as a function of the macroscopic electric field is shown in Figure 10a,c, indicating that bare SiNWs can be turned on at $E_0 = 4.3 \pm 0.1$ V/μm, while the UNCD/SiNW heterostructures exhibit a low threshold field of $E_0 = 3.7 \pm 0.1$ V/μm. Emission current density of bare SiNWs goes as high as ∼0.1 mA/cm^2 at 25 V/μm, whereas the current density for UNCD/SiNW is one order of magnitude higher, reaching ∼2 mA/cm^2 at 25 V/μm and with no saturation yet observed at this field. Table 1 shows the enhanced EFE properties of UNCD/SiNWs as compared to those of UNCD, bare SiNWs, CNTs, and UNCD/CNTs. All these materials exhibit relatively low current densities of 0.1, 0.3, and 0.1 mA/cm^2, respectively. However, by coating the SiNWs and CNTs with UNCD, a synergistic effect comes into action, and the current densities are enhanced in about one order of magnitude. The enhancement in electron field emission properties of UNCD/SiNWs can be attributed to the good electrical contact between the sp^2-terminated UNCD and SiNWs, which facilitates the transfer of electrons from Si to UNCD, thus circumventing the silicon oxide layer. Moreover, the presence of sp^2-hybridized carbon around the diamond crystallites and the geometrical enhancement factor (diameters ∼5−10 nm) also play an important role in facilitating the electron emission process itself. Additionally, the high density of UNCD crystallites is a key parameter influencing the EFE properties. Therefore, the increment of current density can be attributed to the combination of the high density of UNCD particles coating the SiNWs and the high density of the SiNW network.

Table 1. Comparison of Electron Field Emission Properties

material	E_0 (V/μm)[a]	J_{max} (mA/cm^2)[b]	E_{Jmax} (V/μm)[c]	reference
SiNWs	4.3	0.1	25	present work
CNTs	2.3	0.3	7.5	53, 54
UNCD	5.6	0.1	18	34
UNCD/CNTs	1.9	2.0	20	51
UNCD/SiNWs	3.7	2.0	25	present work

[a] E_0: turn-on field. [b] J_{max}: maximum electron field emission current density. [c] E_{Jmax}: field required for J_{max}.

The $\ln(J/E^2) - 1/E$ plots (see Figure 10b,d) describe the exponential dependence relationship between the applied electric field and emission current. The straight lines indicate that the field emission from SiNWs and UNCD/SiNWs follows the Fowler−Nordheim (FN) behavior, represented by the simplified FN equation.

$$J = \frac{A\beta^2E^2}{\phi}\exp\left[\frac{-B\phi^{3/2}}{\beta E}\right] \quad (1)$$

where J is the current density, E the applied field strength, β the field enhancement factor, ϕ the work function of emitter materials, and A and B are constants, corresponding to $A = 1.56 \times 10^{-10}$ AV^2 eV and $B = -6.83 \times 10^3$ V(eV)$^{3/2}$ (μm)$^{-1}$, respectively. The local electric field E_L can be related to the

macroscopic field E_M by $E_L = \beta E_M$, which indicates that high values of β signify high local electric field due to the presence of one-dimensional SiNWs and are enhanced by UNCD coating. Therefore, β is a parameter dependent on the geometry of the nanowire, crystal structure, and density of emitting points and is used to determine the degree of the field emission enhancement. Assuming that the work function of SiNWs is close to 4.7 eV,[55] β can be calculated from the slope of the F−N plot using the expression

$$\beta = -\frac{B\phi^{3/2}}{\text{slope}} \quad (2)$$

For bare SiNWs, the FN plot is fitted with a single slope which corresponds to the β value of ∼1447. The enhancement factor calculated for the two slopes for UNCD/SiNWs corresponds to the β values of ∼1163 at low field and ∼1982 at high field. These β values are superior to those reported by Thomas et al.[26] and much higher than values reported by Tzeng et al.[25,33] whose field emission results and analysis appear to have internal contradictions.

Two emission regimes can be distinguished. In the low-field regime <7 V/μm, electrons are emitted mainly from the sp^2 carbon around the UNCD crystallites that are distributed along the SiNWs. The direct contact between UNCD and Si avoids the barrier of the oxide layer and takes advantage of the negative electron affinity of diamond.[56] The second slope at fields >7 V/μm corresponds to higher local electric fields that are required to obtain emission directly from the SiNWs.

4. CONCLUSION

Ultrananocrystalline diamond coating on silicon nanowires has been done by HFCVD using paraffin wax as a seeding source for the growth of diamond on silicon nanowires. The HRTEM and EELS analyses of the UNCD coating on SiNWs revealed a grain size of 5−10 nm. The fabricated nanostructures have enhanced electron field emission (EFE) properties as compared to the EFE performance of other field emitters, including bare SiNWs and UNCD. The UNCD/SiNWs exhibit turn-on fields around E_0 = 3.7 V/μm and current densities around 2 mA/cm^2 at an applied field of 25 V/μm. It can be concluded that the coating of UNCD on SiNWs greatly influenced their field emission performance. The enhanced electron field emission properties of UNCD/SiNW are ascribed to the synergistic effects of UNCD crystallites and SiNWs. The presence of sp^2-hybridized carbon around the diamond crystallites and the geometrical enhancement factor also play an important role in facilitating the electron emission process.

AUTHOR INFORMATION

Corresponding Author

*E-mail: javier.palomino@upr.edu.

Author Contributions

The manuscript was written through contributions of all authors. All authors have given approval to the final version of the manuscript.

Notes

The authors declare no competing financial interest.

ACKNOWLEDGMENTS

This research was carried out under the auspices of the Institute for Functional Nanomaterials (NSF Grant 1002410), PR NASA EPSCoR (NASA Cooperative Agreement NNX07AO30A), and PR DOE EPSCoR (DOE Grant DE-FG02-08ER46526, J.P.). We gratefully acknowledge the use of research facilities of various researchers at the University of Puerto Rico: Sputtering (Dr. Luis Fonseca); Micro-Raman Spectroscopy (Dr. Ram Katiyar and Mr. William Perez).

REFERENCES

(1) Liu, Z.; Pan, Z.; Sun, L.; Tang, D.; Zhou, W.; Wang, G.; Qian, L.; Xie, S. Synthesis of Silicon Nanowires Using AuPd Nanoparticles Catalyst on Silicon Substrate. *J. Phys. Chem. Solids* **2000**, *61*, 1171−1174.

(2) Morales, A.; Lieber, C. A Laser Ablation Method for the Synthesis of Crystalline Semiconductor Nanowires. *Science* **1998**, *279*, 208−211.

(3) Feng, S. Q.; Yu, D. P.; Zhang, H. Z.; Bai, Z. G.; Ding, Y. The Growth Mechanism of Silicon Nanowires and Their Quantum Confinement Effect. *J. Cryst. Growth* **2000**, *209*, 513−517.

(4) Wagner, R. S.; Ellis, W. C. Vapor-Liquid-Solid Mechanism of Single Crystal Growth. *Appl. Phys. Lett.* **1964**, *4*, 89−90.

(5) Q. Peng, K.; P. Huang, Z.; Zhu, J. Fabrication of Large-Area Silicon Nanowire p−n Junction Diode Arrays. *Adv. Mater.* **2004**, *16*, 73−76.

(6) Iijima, S. Helical Microtubules of Graphitic Carbon. *Nature* **1991**, *354*, 56−58.

(7) Rinzler, A. G.; Hafner, J. H.; Nikolaev, P.; Nordlander, P.; Colbert, D. T.; Smalley, R. E.; Lou, L.; Kim, S. G.; Tománek, D. Unraveling Nanotubes: Field Emission from an Atomic Wire. *Science* **1995**, *269*, 1550−1553.

(8) Chen, K.; Deng, J.; Zhao, F.; Cheng, G.; Zheng, R. Influence of Zn Ion Implantation on Structures and Field Emission Properties of Multi-Walled Carbon Nanotube Arrays. *Sci. China: Technol. Sci.* **2010**, *53*, 776−781.

(9) Lee, N. S.; Chung, D. S.; Han, I. T.; Kang, J. H.; Choi, Y. S.; Kim, H. Y.; Park, S. H.; Jin, Y. W.; Yi, W. K.; Yun, M. J.; Jung, J. E.; Lee, C. J.; You, J. H.; Jo, S. H.; Lee, C. G.; Kim, J. M. Application of Carbon Nanotubes to Field Emission Displays. *Diamond Relat. Mater.* **2001**, *10*, 265−270.

(10) Biaggi-Labiosa, A.; Solá, F.; Resto, O.; Fonseca, L. F.; González-Berríos, A.; De Jesús, J.; Morell, G. Nanocrystalline Silicon as the Light Emitting Material of a Field Emission Display Device. *Nanotechnology* **2008**, *19*, 225202.

(11) Zhu, Y. W.; Zhang, H. Z.; Sun, X. C.; Feng, S. Q.; Xu, J.; Zhao, Q.; Xiang, B.; Wang, R. M.; Yu, D. P. Efficient Field Emission from ZnO Nanoneedle Arrays. *Appl. Phys. Lett.* **2003**, *83*, 144−146.

(12) Xiang, B.; Zhang, Y.; Wang, Z.; Luo, X. H.; Zhu, Y. W.; Zhang, H. Z.; Yu, D. P. Field-Emission Properties of TiO2 Nanowire Arrays. *J. Phys. D: Appl. Phys.* **2005**, *38*, 1152−1155.

(13) Wu, Z. S.; Deng, S. Z.; Xu, N. S.; Chen, J.; Zhou, J.; Chen, J. Needle-Shaped Silicon Carbide Nanowires: Synthesis and Field Electron Emission Properties. *Appl. Phys. Lett.* **2002**, *80*, 3829−3831.

(14) Chen, J.; Deng, S. Z.; Xu, N. S.; Wang, S.; Wen, X.; Yang, S.; Yang, C.; Wang, J.; Ge, W. Field Emission from Crystalline Copper Sulphide Nanowire Arrays. *Appl. Phys. Lett.* **2002**, *80*, 3620−3622.

(15) Valentín, L. A.; Carpena-Nuñez, J.; Yang, D.; Fonseca, L. F. Field Emission Properties of Single Crystal Chromium Disilicide Nanowires. *J. Appl. Phys.* **2013**, *113*, 014308−1−014308−5.

(16) Huang, C. T.; Hsin, C. L.; Huang, K. W.; Lee, C. Y.; Yeh, P. H.; Chen, U. S.; Chen, L. J. Er-Doped Silicon Nanowires with 1.54 Mm Light-Emitting and Enhanced Electrical and Field Emission Properties. *Appl. Phys. Lett.* **2007**, *91*, 093133−1−093133−3.

(17) Kulkarni, N. N.; Bae, J.; Shih, C.-K.; Stanley, S. K.; Coffee, S. S.; Ekerdt, J. G. Low-Threshold Field Emission from Cesiated Silicon Nanowires. *Appl. Phys. Lett.* **2005**, *87*, 213115−1−213115−3.

(18) Au, F. C. K.; Wong, K. W.; Tang, Y. H.; Zhang, Y. F.; Bello, I.; Lee, S. T. Electron Field Emission from Silicon Nanowires. *Appl. Phys. Lett.* **1999**, *75*, 1700−1702.

(19) Ha, J. K.; Chung, B. H.; Han, S. Y.; Choi, J. O. Drastic Changes in the Field Emission Characteristics of a Mo-Tip Field Emitter Array

Having PH_3-Doped a-Si:H as a Resistive Layer Material throughout Vacuum Packaging Processes in a Field Emission Display. *J. Vac. Sci. Technol., B: Nanotechnol. Microelectron.: Mater., Process., Meas., Phenom.* **2002**, *20*, 2080−2084.
(20) Ok, Y.-W.; Seong, T.-Y.; Choi, C.-J.; Tu, K. N. Field Emission from Ni-Disilicide Nanorods Formed by Using Implantation of Ni in Si Coupled with Laser Annealing. *Appl. Phys. Lett.* **2006**, *88*, 0431061−0431063.
(21) Chen, T.-M.; Hung, J.-Y.; Pan, F.-M.; Chang, L.; Wu, S.-C.; Tien, T.-C. Pulse Electrodeposition of Iridium Oxide on Silicon Nanotips for Field Emission Study. *J. Nanosci. Nanotechnol.* **2009**, *9*, 3264−3268.
(22) Zhao, F.; Cheng, G.-A.; Zheng, R.-T.; Zhao, D.-D.; Wu, S.-L.; Deng, J.-H. Field Emission Enhancement of Au-Si Nano-Particle-Decorated Silicon Nanowires. *Nanoscale Res. Lett.* **2011**, *6*, 176−1−176−5.
(23) She, J. C.; Huq, S. E.; Chen, J.; Deng, S. Z.; Xu, N. S. Comparative Study of Electron Emission Characteristics of Silicon Tip Arrays with and without Amorphous Diamond Coating. *J. Vac. Sci. Technol. B: Nanotechnol. Microelectron.: Mater., Process., Meas., Phenom.* **1999**, *17*, 592−595.
(24) Liu, J.; Zhirnov, V. V.; Wojak, G. J.; Myers, A. F.; Choi, W. B.; Hren, J. J.; Wolter, S. D.; McClure, M. T.; Stoner, B. R.; Glass, J. T. Electron Emission from Diamond Coated Silicon Field Emitters. *Appl. Phys. Lett.* **1994**, *65*, 2842−2844.
(25) Tzeng, Y.-F.; Liu, K.-H.; Lee, Y.-C.; Lin, S.-J.; Lin, I.-N.; Lee, C.-Y.; Chiu, H.-T. Fabrication of an Ultra-Nanocrystalline Diamond-Coated Silicon Wire Array with Enhanced Field-Emission Performance. *Nanotechnology* **2007**, *18*, 435703−1−435703−5.
(26) Thomas, J. P.; Chen, H.-C.; Tseng, S.-H.; Wu, H.-C.; Lee, C.-Y.; Cheng, H. F.; Tai, N.-H.; Lin, I.-N. Preferentially Grown Ultrananno c-Diamond and N-Diamond Grains on Silicon Nanoneedles from Energetic Species with Enhanced Field-Emission Properties. *ACS Appl. Mater. Interfaces* **2012**, *4*, 5103−5108.
(27) Himpsel, F.; Knapp, J.; VanVechten, J.; Eastman, D. Quantum Photoyield of diamond(111)—A Stable Negative-Affinity Emitter. *Phys. Rev. B: Condens. Matter Mater. Phys.* **1979**, *20*, 624−627.
(28) Lu, X.; Yang, Q.; Chen, W.; Xiao, C.; Hirose, A. Field Electron Emission Characteristics of Diamond Films with Different Grain Morphologies. *J. Vac. Sci. Technol., B: Nanotechnol. Microelectron.: Mater., Process., Meas., Phenom.* **2006**, *24*, 2575−2580.
(29) Okano, K.; Koizumi, S.; Silva, S. R. P.; Amaratunga, G. A. J. Low-Threshold Cold Cathodes Made of Nitrogen-Doped Chemical-Vapour-Deposited Diamond. *Nature* **1996**, *381*, 140−141.
(30) Wang, Z. L.; Luo, Q.; Li, J. J.; Wang, Q.; Xu, P.; Cui, Z.; Gu, C. Z. The High Aspect Ratio Conical Diamond Tips Arrays and Their Field Emission Properties. *Diamond Relat. Mater.* **2006**, *15*, 631−634.
(31) Liu, J. Field Emission Characteristics of Diamond Coated Silicon Field Emitters. *J. Vac. Sci., Technol. B: Microelectron. Nanometer Struct.–Process., Meas., Phenom.* **1995**, *13*, 422−426.
(32) Kiselev, N. A.; Hutchison, J. L.; Roddatis, V. V.; Stepanova, A. N.; Aksenova, L. L.; Rakova, E. V.; Mashkova, E. S.; Molchanov, V. A.; Givargizov, E. I. TEM and HREM of Diamond Crystals Grown on Si Tips: Structure and Results of Ion-Beam-Treatment. *Micron* **2005**, *36*, 81−88.
(33) Tzeng, Y.-F.; Lee, C.-Y.; Chiu, H.-T.; Tai, N.-H.; Lin, I.-N. Electron Field Emission Properties on Ultra-Nano-Crystalline Diamond Coated Silicon Nanowires. *Diamond Relat. Mater.* **2008**, *17*, 1817−1820.
(34) Varshney, D.; Palomino, J.; Gil, J.; Resto, O.; Weiner, B. R.; Morell, G. New Route to the Fabrication of Nanocrystalline Diamond Films. *J. Appl. Phys.* **2014**, *115*, 054304−1−054304−6.
(35) Auciello, O.; Sumant, A. V. Status Review of the Science and Technology of Ultrananocrystalline Diamond (UNCD) Films and Application to Multifunctional Devices. *Diamond Relat. Mater.* **2010**, *19*, 699−718.
(36) Morell, G.; González-Berríos, a.; Weiner, B. R.; Gupta, S. Synthesis, Structure, and Field Emission Properties of Sulfur-Doped Nanocrystalline Diamond. *J. Mater. Sci.: Mater. Electron.* **2006**, *17*, 443−451.
(37) Niu, J.; Sha, J.; Yang, Q.; Yang, D. Crystallization and Raman Shift of Array-Orderly Silicon Nanowires after Annealing at High Temperature. *Jpn. J. Appl. Phys.* **2004**, *43*, 4460−4461.
(38) Meier, C.; Lüttjohann, S.; Kravets, V. G.; Nienhaus, H.; Lorke, A.; Wiggers, H. Raman Properties of Silicon Nanoparticles. *Phys. E (Amsterdam, Neth.)* **2006**, *32*, 155−158.
(39) Dhara, S.; Giri, P. K. Effect of Growth Temperature on the Catalyst-Free Growth of Long Silicon Nanowires Using Radio Frequency Magnetron Sputtering. *Int. J. Nanosci.* **2011**, *10*, 13−17.
(40) Liu, Z. .; Xie, S. .; Zhou, W. .; Sun, L. .; Li, Y. .; Tang, D. .; Zou, X. .; Wang, C. .; Wang, G. Catalytic Synthesis of Straight Silicon Nanowires over Fe Containing Silica Gel Substrates by Chemical Vapor Deposition. *J. Cryst. Growth* **2001**, *224*, 230−234.
(41) Wang, X.; Ocola, L. E.; Divan, R. S.; Sumant, A. V. Nanopatterning of Ultrananocrystalline Diamond Nanowires. *Nanotechnology* **2012**, *23*, 075301−1−075301−7.
(42) Maillard-Schaller, E.; Kuettel, O. M.; Diederich, L.; Schlapbach, L.; Zhirnov, V. V.; Belobrov, P. I. Surface Properties of Nanodiamond Films Deposited by Electrophoresis on Si(100). *Diamond Relat. Mater.* **1999**, *8*, 805−808.
(43) Xiao, X.; Birrell, J.; Gerbi, J. E.; Auciello, O.; Carlisle, J. A. Low Temperature Growth of Ultrananocrystalline Diamond. *J. Appl. Phys.* **2004**, *96*, 2232−2239.
(44) Varshney, D.; Kumar, A.; Guinel, M. J.-F.; Weiner, B. R.; Morell, G. Spontaneously Detaching Self-Standing Diamond Films. *Diamond Relat. Mater.* **2012**, *21*, 99−102.
(45) Suzuki, M.; Kudoh, Y.; Homma, Y.; Kaneko, R. Monoatomic Step Observation on Si(111) Surfaces by Force Microscopy in Air. *Appl. Phys. Lett.* **1991**, *58*, 2225−2227.
(46) Shakerzadeh, M.; Teo, E. H. T.; Sorkin, A.; Bosman, M.; Tay, B. K.; Su, H. Plasma Density Induced Formation of Nanocrystals in Physical Vapor Deposited Carbon Films. *Carbon N. Y.* **2011**, *49*, 1733−1744.
(47) Chen, H.-C.; Chen, S.-S.; Wang, W.-C.; Lee, C.-Y.; Guo, J.; Lin, I.-N.; Chang, C.-L. The Potential Application of Ultra-Nanocrystalline Diamond Films for Heavy Ion Irradiation Detection. *AIP Adv.* **2013**, *3*, 062113−1−062113−20.
(48) Chen, Y. C.; Zhong, X. Y.; Konicek, A. R.; Grierson, D. S.; Tai, N. H.; Lin, I. N.; Kabius, B.; Hiller, J. M.; Sumant, A. V.; Carpick, R. W.; Auciello, O. Synthesis and Characterization of Smooth Ultra-nanocrystalline Diamond Films via Low Pressure Bias-Enhanced Nucleation and Growth. *Appl. Phys. Lett.* **2008**, *92*, 133113−1−133113−3.
(49) Schmidt, V.; Wittemann, J. V.; Senz, S.; Gösele, U. Silicon Nanowires: A Review on Aspects of Their Growth and Their Electrical Properties. *Adv. Mater.* **2009**, *21*, 2681−2702.
(50) Klimovskaya, A.; Sarikov, A.; Pedchenko, Y.; Voroshchenko, A.; Lytvyn, O.; Stadnik, A. Study of the Formation Processes of Gold Droplet Arrays on Si Substrates by High Temperature Anneals. *Nanoscale Res. Lett.* **2011**, *6*, 151.
(51) Varshney, D.; Sumant, A. V.; Resto, O.; Mendoza, F.; Quintero, K. P.; Ahmadi, M.; Weiner, B. R.; Morell, G. Single-Step Route to Hierarchical Flower-like Carbon Nanotube Clusters Decorated with Ultrananocrystalline Diamond. *Carbon N. Y.* **2013**, *63*, 253−262.
(52) Chen, L.-J.; Tai, N.-H.; Lee, C.-Y.; Lin, I.-N. Effects of Pretreatment Processes on Improving the Formation of Ultra-nanocrystalline Diamond. *J. Appl. Phys.* **2007**, *101*, 064308−1−064308−6.
(53) Katar, S.; Labiosa, A.; Plaud, A. E.; Mosquera-Vargas, E.; Fonseca, L.; Weiner, B. R.; Morell, G. Silicon Encapsulated Carbon Nanotubes. *Nanoscale Res. Lett.* **2009**, *5*, 74−80.
(54) Katar, S. L.; González-Berríos, A.; De Jesus, J.; Weiner, B.; Morell, G. Direct Deposition of Bamboo-Like Carbon Nanotubes on Copper Substrates by Sulfur-Assisted HFCVD. *J. Nanomater.* **2008**, *2008*, 515890−1−515890−7.
(55) Minami, T.; Miyata, T.; Yamamoto, T. Work Function of Transparent Conducting Multicomponent Oxide Thin Films Prepared

by Magnetron Sputtering. *Surf. Coat. Technol.* **1998**, *108−109*, 583−587.
(56) Liao, M.; Zhang, Z.; Wang, W.; Liao, K. Field-Emission Current from Diamond Film Deposited on Molybdenum. *J. Appl. Phys.* **1998**, *84*, 1081−1084.